Physics in Medicine &
Biology

In silico neutron relative biological effectiveness estimations for pre-DNA repair and post-DNA repair endpoints

To cite this article before publication: Nicolas Desjardins-Proulx *et al* 2026 *Phys. Med. Biol.* in press https://doi.org/10.1088/1361-6560/ae36e1

In silico Neutron Relative Biological Effectiveness Estimations For Pre-DNA Repair And Post-DNA Repair Endpoints

Nicolas Desjardins[1], John Kildea[1]

[1]Medical Physics Unit, McGill University, Montreal, QC, H4A3J1, Canada

E-mail: nicolas.desjardins-proulx@mail.mcgill.ca

Abstract.

A comprehensive understanding of the energy-dependent stochastic risks associated with neutron exposure is crucial to develop robust radioprotection systems. However, the scarcity of experimental data presents significant challenges in this domain. Track-structure Monte Carlo simulations with DNA models have demonstrated their potential to further our fundamental understanding of neutron-induced stochastic risks. To date, most track-structure Monte Carlo studies on the relative biological effectiveness (RBE) of neutrons have focused on various types of DNA damage clusters defined using base pair distances. In this study, we extend these methodologies by incorporating the simulation of non-homologous end joining (NHEJ) DNA repair in order to evaluate the RBE of neutrons for misrepairs. To achieve this, we adapted our previously published Monte Carlo DNA damage simulation pipeline, which combines condensed-history and track-structure Monte Carlo methods, to support the standard DNA damage (SDD) data format. This adaptation enabled seamless integration of neutron-induced DNA damage results with the DNA Mechanistic Repair Simulator (DaMaRiS) toolkit. Additionally, we developed a clustering algorithm that reproduces pre-repair endpoints studied in prior works, as well as novel damage clusters based on Euclidean distances. The neutron RBE for misrepairs obtained in this study exhibits a qualitatively similar shape as the RBE obtained for previously reported pre-repair endpoints. However, it peaks higher, reaching a maximum RBE value of 23(1) at a neutron energy of 0.5 MeV. Furthermore, we found that misrepair outcomes were better reproduced using the pre-repair endpoint defined with the Euclidean distance between double-strand breaks rather than with previously published pre-repair endpoints based on base-pair distances. The optimal maximal Euclidean distances were 18 nm for 0.5 MeV neutrons and 60 nm for 250 keV photons. Although this may indicate that Euclidean-distance–based DSB clustering more accurately reflects the DNA damage configurations that lead to misrepairs, the fact that neutrons and photons require different distances raises doubts on whether a single, universal pre-repair endpoint can used as a stand-in for larger-scale aberrations across all radiation qualities.

1 Introduction

1.1 Motivations

Neutron radiation exposure is a potential concern in radiotherapy with high-energy photon beams (Howell *et al* 2006), in particle therapy (Schneider and Hälg 2015), and in certain occupational environments such as in air travel (Goldhagen 2000) and in space travel (Stricklin *et al* 2021). The stochastic risks associated with neutron exposure are known to be highly energy dependent (ICRP 2003); however, quantification of this energy dependence is challenging due to the scarcity of suitable human exposure data sets (Ottolenghi *et al* 2013).

Practically, the stochastic risks of neutrons are quantified by scaling the better-known risks associated with x-rays and gamma rays, for which there is a more substantial body of literature. This approach assumes that the effects of neutrons and photons are qualitatively the same but quantitatively different. In the modern internationally-established system of protection against radiation exposure, as promulgated by the International Commission for Radiological Protection (ICRP) and the US Nuclear Regulatory Commission (NRC), these scaling factors are the radiation weighting factor w_{R} (ICRP 2007) and the quality factor Q (US NRC 2021), respectively. The values of w_{R} and Q for neutrons were agreed on by their respective agencies based on the results of various radiobiological studies using the relative biological effectiveness (RBE) formalism.

The RBE is an endpoint-specific metric that compares the effect of a given radiation quality, defined by its particle type and energy, to that of a reference radiation, which is typically 250 kVp x-rays, ^{60}Co γ-rays, or ^{137}Cs γ-rays . The RBE of a radiation quality i is defined as the dose ratio

$$\mathrm{RBE} = \frac{D_r}{D_i}, \tag{1}$$

where D_r is the dose of a reference radiation, and D_i is the dose of a radiation quality of interest i that produces the same biological endpoint (e.g., number of chromosome aberrations) (CIRRPC 1995).

For simplicity, w_{R} and Q are assumed to be independent of endpoint, dose, and dose rate, and the factors for photons of all energies are set to unity. This; however, does not reflect the complexity of neutron RBE, which depends on those aforementioned quantities. For certain biological endpoints, the non-linearity of the photon dose–response curve also implies that the RBE of neutrons depends on both dose and dose rate. Furthermore, the biological efficacy of photons is weakly energy dependent, which complicates the comparison of RBE results based on different reference photons.

Ultimately, the difference in biological effectiveness of different radiation qualities for the same absorbed dose is understood to be the result of the difference in their energy deposition patterns. In the case of neutrons and photons, which are both indirectly ionizing particles, this translates into a difference in the energy deposition patterns of their respective charged secondary particles.

In human tissue or, even simpler, in a 4-element tissue equivalent material (Lund *et al* 2020), the secondary particle field of neutrons varies widely with neutron energy. The relative abundances of the particle types within the field change, the spectra of those particles change, and the relative dose contributions of each particle type change. On the scale of a human being, this also leads to significant variation of neutron RBE with depth as a result of continuous neutron moderation.

1.2 Prior work

Various studies (Baiocco *et al* 2016, Lund *et al* 2020, Montgomery *et al* 2021, Manalad *et al* 2023, Mentana *et al* 2025) have demonstrated that Monte Carlo simulations can reproduce key features of the energy dependence of neutron-induced stochastic risks from first principles. These studies employed a methodology that couples condensed-history and track-structure simulations. Condensed-history Monte Carlo (CHMC) simulations make it computationally feasible to capture changes in the secondary particle field of neutrons at the scale of a human, and to do so in materials other than water, to which track-structure Monte Carlo (TSMC) simulations are otherwise typically confined (Lund *et al* 2020). In contrast, TSMC simulations provide the level of detail necessary to investigate energy deposition at subcellular scales.

More concretely, the methodology employed in these studies involved using CHMC simulations to determine the relative dose contributions and energy spectra of the various secondary particle species produced by neutrons, as a function of neutron energy and depth in the medium. The secondary particle spectra were then sampled to perform TSMC simulations aimed at investigating various endpoints for neutron RBE estimation. Lund *et al* (2020) provided RBE estimates based on the mean lineal energy, Montgomery *et al* (2021) and Manalad *et al* (2023) provided RBE estimates for explicit DNA lesions, and Baiocco *et al* (2016) did both.

The aforementioned three studies that scored DNA lesions used molecular DNA models with scoring units representing the individual components of nucleotides: the phosphate group, sugar and nitrogenous base. Together, these studies provided RBE estimates for various types of DNA lesions that are highly likely to result in misrepairs, which are considered an early step in the development of carcinogenesis (Jeggo and Löbrich 2007).

Another notable study is that of Zabihi *et al* (2020), which also investigated neutron-induced DNA damage with TSMC. Importantly, Zabihi *et al* (2020) investigated the interaction of two DSBs to simulate the formation of misrepairs. Their simulations; however, did not include indirect action of radiation; that is, the interaction with DNA of the free radicals produced by radiolysis, which was included in the work of Manalad *et al* (2023) and Baiocco *et al* (2016).

1.3 Objective 1

The first objective of this study was to compare how the neutron RBE for misrepairs resulting from both the direct and indirect action compares to that of the pre-repair endpoints presented in the works of Baiocco *et al* (2016) and Manalad *et al* (2023), which looked at various types of DSB clusters defined using base pair distances.

In order to achieve this goal, we adapted our previously published neutron-induced DNA damage simulation pipeline (Manalad *et al* 2023) to output the Standard DNA Damage (SDD) Data Format (Schuemann *et al* 2019b), making it compatible with the DNA Mechanistic Repair Simulator (DaMaRiS) toolkit (Warmenhoven *et al* 2019).

Furthermore, we wrote a Python script that reproduces the pre-repair endpoints presented in the works of Baiocco *et al* (2016) and Manalad *et al* (2023) from the SDD file in order to compare the RBE for misrepairs and pre-repair endpoints while keeping everything else consistent.

1.4 Objective 2

Two DSBs can be many base pairs away from each other or even on different chromosomes, but because of the high level of compaction of the DNA, they can still be within short Euclidean distances of each other, making the DSB pair a potential source of misrepair. Motivated by this, the second objective of this study was to determine the RBE for DSB clusters based on Euclidean distances. To achieve this, the aforementioned Python script also computes the yield of this new endpoint from the SDD file.

1.5 RBE for linear dose responses

We end this Introduction with a few words on the RBE formalism. Provided that both the radiation type of interest and the reference radiation have a linear dose response for the endpoint and dose range relevant to the RBE calculation, the RBE is a dose independent quantity. For linear dose response, we have isoeffect when

$$\alpha_i D_i = \alpha_r D_r, \tag{2}$$

where α_i and α_r are the linear coefficients of the dose responses of the radiation type of interest and the reference radiation respectively. From (1) and (2) we get

$$\mathrm{RBE} = \frac{\alpha_i}{\alpha_r}. \tag{3}$$

Conveniently, in the case where $D_i = D_r = D$, then (3) can be rewritten as

$$\mathrm{RBE} = \frac{\alpha_i D}{\alpha_r D} = \frac{Y_i}{Y_r}, \tag{4}$$

where Y_i and Y_r are the yields of the endpoint of interest. This quantity is typically referred as the radiation effect ratio (RER) and is equivalent to the RBE for linear dose responses. Given that the dose response of all endpoints of interest for this study were found to be linear within the dose range of interest, that is, at least up to 20 Gy, we obtained the RBE by computing the RER for 1 Gy, consistent with the work of Baiocco *et al* (2016), Montgomery *et al* (2021), Manalad *et al* (2023) and Mentana *et al* (2025). At higher doses, beyond the range explored in this study, one could expect a quadratic contribution in the dose response arising from interactions between damage events from independent tracks, which is the usual rationale for the beta component in the linear–quadratic model.

2 Methods

2.1 Overview

The simulation pipeline can be broken down into four components. The first component is a series of CHMC simulations conducted to acquire the energy and relative dose contributions of the secondary particles released in tissue by neutrons and photons, see Figure 1 a). The second component is a series of TSMC simulations with a cell nucleus model performed to score various basic DNA lesions in the SDD format, see Figure 1 b). The resulting SDD files are then directly processed by a Python script to obtain pre-repair endpoints, see Figure 1 c), or fed into DaMaRiS to obtain misrepair outcomes, see Figure 1 d).

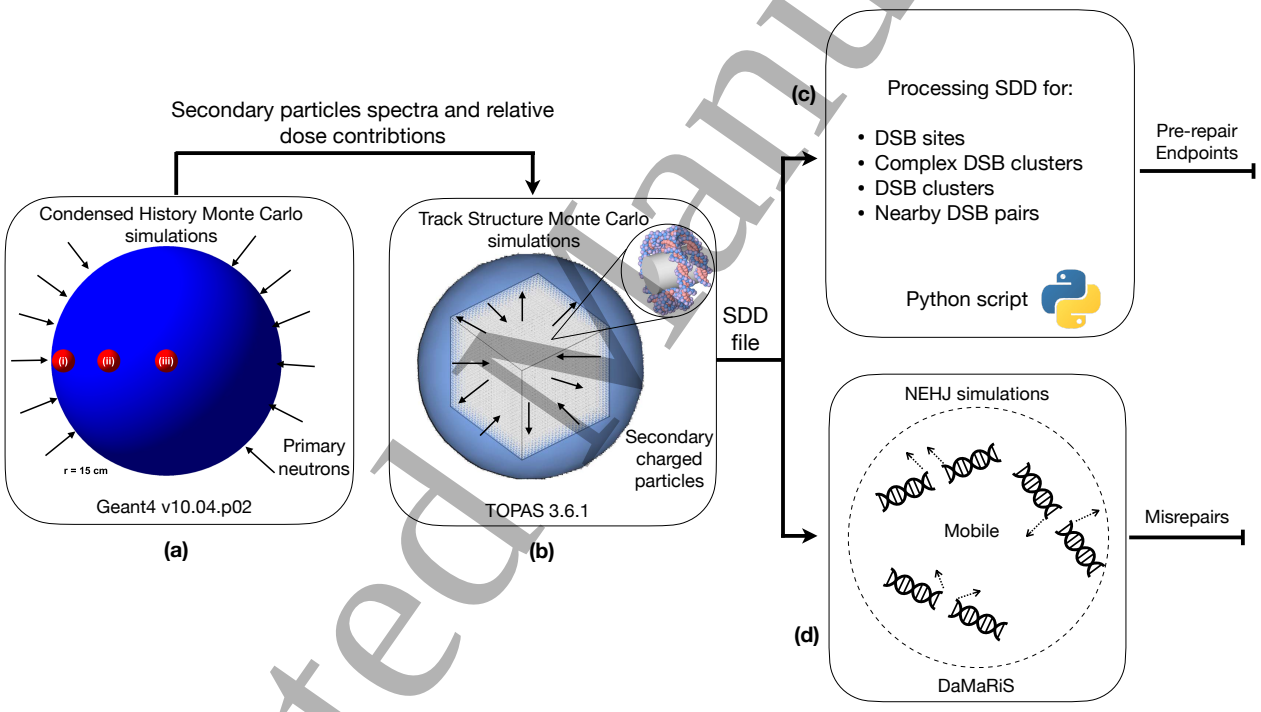

Figure 1: a) CHMC component with a 30 cm ICRU-4 sphere. The smaller red spheres are the scoring volumes. Only the outer scoring volume (i) is used for this work it has a radius of 1.5 cm and is centered 1.5 cm away from the surface. b) TSMC component with a nucleus model. The source is obtained sampling the secondary particle spectra from a). c) Python script that computes the pre-repair endpoints yields from the SDD file. d) Depiction of the mobile DSB ends in the spherical boundary with a diamater of 13.51 µm. The figure of the ICRU-4 sphere a) and the nucleus model with the octameter in the zoomed circle are modified illustrations reproduced from Montgomery *et al* (2021)

2.2 Condensed-history simulations

This aspect of the methodology has been detailed in our previous publication (Lund *et al* 2020), so we provide only a brief overview here. The goal of the CHMC simulations was to characterize the spectra and relative dose contributions of the various secondary particles generated by primary neutrons and photons as they pass through biological tissues. The simulations were carried out with monoenergetic neutron sources, covering 18 energies ranging from 1 eV to 10 MeV, and a single photon source of 250 keV, which served as the reference energy for our RBE calculations. These simulations were conducted using Geant4 v10.04.p02 and its radiobiology extension Geant4-DNA (Incerti *et al* 2010a) with an ICRU-4 sphere (White *et al* 1989), which has a diameter of 30 cm.

The neutron source used was inversely isotropic; that is, neutrons were uniformly distributed over a large surrounding sphere and directed toward the center of the ICRU-4 sphere. This setup was designed to reproduce a non-directional, total-body exposure. Consequently, the sampling obtained by a scoring volume depends only on its distance from the center of the 30 cm ICRU-4 sphere, and not on its specific position relative to the source, as would be the case for a mono-directional beam.

Because the spectrum and the relative dose contribution of each secondary particle species is expected to change with depth in the medium, in the work of Lund *et al* (2020) three depths were sampled in the ICRU-4 sphere. This sampling was done with three scoring volumes which are depicted in Figure 1. The scoring volumes are just delimitation within the 30 cm ICRU-4 sphere, and thus, are made of the same material.

Only the outer scoring volume will be considered in this study as it provides the maximal RBE. This aligns with the conservative approach adopted by the radiation protection agencies. The outer scoring volume is positioned a the very edge of the 30 cm ICRU sphere, it is the red sphere (i) in Figure 1. It has radius of 1.5 cm and is therefore centered at a depth of 1.5 cm from the ICRU-4 sphere's surface.

The secondary particle species released by neutrons are numerous but because of limitations in the current Geant4-DNA physics list for the required energy range (Incerti *et al* 2016), only the secondary electrons, protons, and alpha particles were considered in the next step. The relative dose contribution of those three particle species were renormalized to sum to unity.

2.3 Radiation-induced DNA damage simulations

The TSMC DNA damage simulations were conducted using the DNA model and a modified version of the scorer employed in our previous studies on complex DSB lesions (Montgomery *et al* 2021, Manalad *et al* 2023). The scorer, which was made as a TOPAS (Perl *et al* 2012) class, was modified to output DNA lesions in the SDD Format; however, all parameters pertaining to scoring lesions were left unmodified; therefore, the previous benchmarking conducted with mononenergetic protons and presented in Manalad *et al* (2023) remains applicable to this work.

Compared to our previous work (Montgomery *et al* 2021, Manalad *et al* 2023), a different

Table 1: Track-structure DNA damage simulations parameters

Parameter	Values
Physics Module	G4EmDNAPhysics_hybrid2and4 Combination of G4EmDNAPhysics_option2 and G4EmDNAPhysics_option4
Strand break energy threshold	17.5 eV
Base lesion energy threshold	17.5 eV
Probability of $HO^{\bullet}$ to cause damage	40 %
DSB max length	10 bp
Target dose	1 Gy
Number of repeated simulations	100 for neutron secondaries, 950 for photons

TOPAS source parameter was used to specify the neutron secondary particle spectrum. The setting (s:So/Example/BeamEnergySpectrumType = 'Continuous') was applied instead of (s:So/Example/BeamEnergySpectrumType = 'Discrete'). This change allows particles to be generated anywhere within the energy bin width of the particle energy spectrum as opposed to only the edge of the bin. The effect of this change on the pre-repair RBE estimation was evaluated. Other relevant simulation parameters can be found in Table 1.

2.4 DNA repair simulations

For the DNA repair simulations, we used DaMaRiS, a software developed by the PRECISE group at the University of Manchester that has been integrated to TOPAS-nBio (Henthorn *et al* 2018, Ingram *et al* 2019, Warmenhoven *et al* 2019). Briefly, DaMaRiS is a flexible tool that allows one to explore various user-defined repair pathways by defining various repair stages with their associated time constants. The repair pathway dictates the possible progression of the simulation's "objects", such as "DSB end objects" and "synaptic complex objects." For this study, we used the NEHJ pathway provided in TOPAS-nBio and described in Warmenhoven *et al* (2019), with the default allowed repair time of 24 h. We selected the NEHJ only pathway as opposed to the combined NEHJ and HR pathway because our nucleus model best represents the state of a cell in the G0/G1 phase where HR is not available. DaMaRiS confines the moving DSB ends within a spherical reflective boundary. To accommodate our cubic cell nucleus model (Montgomery *et al* 2021), we used its circumscribed sphere as the simulation boundary, that is, a sphere with a radius of 6.755 µm.

2.5 Pre-repair and post-repair endpoints

The RBE is highly dependent on the endpoint being investigated. As stated in the introduction, one goal of this study was to compute various pre-repair endpoints reported in the literature, allowing for comparisons across endpoints while keeping other factors, such as the DNA model and scorer, constant. Additionally, this approach enables the evaluation of similarities in outcomes between our model and other models for the same endpoints.

A description of all endpoints investigated in this study can be found in Table 2. The two new endpoints presented here are the misrepair and the nearby DSB pair. Misrepairs are obtained with DaMaRiS, they include any DSB end that joined to the DSB end from a different DSB site. The two wrongly joined ends can originate from DSBs from the same chromosome or from different chromosomes. Nearby DSB pairs are pre-repair endpoints computed from the SDD file. They are defined as two DSBs within a specified Euclidean distance, measured between their centerpoints. Again, those two DSBs can be on the same chromosome or on different chromosomes. One DSB can be part of more than one nearby DSB pair.

For each neutron energy and for the reference radiation, we conducted the DNA damage simulations pertaining to each secondary particle species independently. Hence, we combined species-specific damage yields via a weighted sum. The yield Y for a primary particle P of a given endpoint is obtained as follows:

$$Y_P = \sum_S \frac{Y_S D_S}{d_S}, \tag{5}$$

where S corresponds to the secondary particle species, d_S corresponds to the relative dose contribution of S obtained from the CHMC simulations, and D_S corresponds to the actual dose deposited by that species in a given TSMC simulation run. Note that for (P = neutron) we have ($S = \{e^-, p^+, \alpha\}$) and for (P = photon) we have ($S = \{e^-\}$). The neutron energy-dependent RBE(E) can be obtained using:

$$\mathrm{RBE}(E) = \frac{Y_n(E)}{Y_X} \tag{6}$$

Table 2: Descriptions of the endpoints used for RBE estimation in this work.

Endpoint name	Description	Minimum number of basic lesions
Pre-repair endpoints		
DSB site	Location of one DSB	2
Complex DSB lesion (Montgomery *et al* 2021) (Manalad *et al* 2023)	Site with a least one DSB and at least one other lesion of any kind where each lesion is within 40 bp of its closest neighbour	3
DSB cluster (Baiocco *et al* 2016)	Site with at least two DSBs within 25 bp	4
Nearby DSB pairs	Two DSBs where the centerpoints of the two DSBs are within a specified Euclidean distance	4
Post-repair endpoints		
Misrepairs	Two DSBs end originating from distinct DSBs that joined together due to a DNA repair mechanism.	4

* In (Montgomery *et al* 2021, Manalad *et al* 2023) this type of lesion is referred to as a complex DSB cluster. To avoid confusion with lesions that require at least two DSBs, called DSB clusters in Baiocco *et al* (2016), we refer to it as a Complex DSB lesion in this work.

3 Results

3.1 Dose response linearity

To examine the linearity of the endpoints considered in this study, we plotted in Figure 2 the dose–response curves for DSB pairs while varying the maximum allowed Euclidean distance from 11 nm to 300 nm, as well as the dose–response curve for photon-induced misrepairs. As shown in Figure 2, increasing the maximum permitted separation between elements of a DNA damage cluster leads to a progressively more nonlinear dose response, since larger distances allow a greater contribution from inter-track interactions.

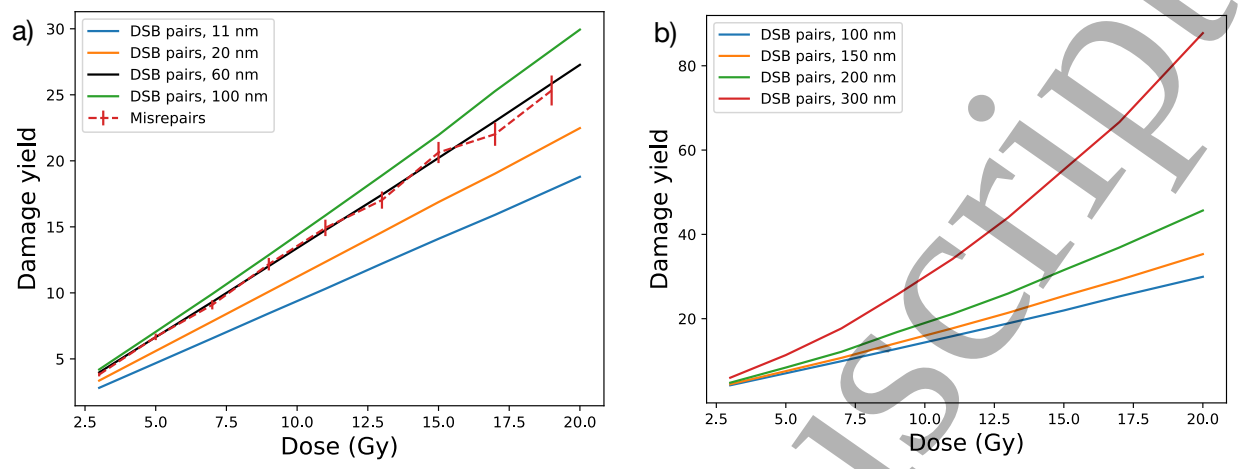

Figure 2: Pre-repair and post-repair damage yield dose response for 250 keV photons from 3 Gy to 20 Gy. a) Dose response for DSB pairs with Euclidean distances in the 11-100 nm range and misrepairs. b) Dose response for DSB pairs with Euclidean distances in the 100-300 nm range.

3.2 Comparing pre-repair endpoints

Applying our Python clustering script to the SDD files resulting from our DNA damage simulations, we computed the RBE for the pre-repair endpoints investigated in Baiocco *et al* (2016), Manalad *et al* (2023), Mentana *et al* (2025), which are described in Table 2. In Figure 3, we compare our results to the RBE values from those studies. The endpoints a) DSB sites, b) Complex DSB lesions, and c) DSB clusters are presented in order of increasing minimum required basic lesions (see Table 2). The maximal RBE for each endpoint obtained in this study is a) 2.54(3), b) 4.78(8), and c) 16(1).

The overall methodology employed in Baiocco *et al* (2016) is similar to the one presented here. Their CHMC simulations were performed using the general-purpose Monte Carlo particle transport code PHITS (Sato *et al* 2013), and their TSMC simulations were carried out with the biophysical simulation tool PARTRAC (Friedland *et al* 2011). The geometry adopted in their CHMC simulations is identical to that used in our study; however, they implemented a different G0/G1 nucleus model. Moreover, instead of using a monoenergetic reference radiation, they used the x-ray spectrum of an Xstrahl-200 unit (220 kV, 2 mm Cu filtration).

Mentana *et al* (2025) likewise used PHITS and PARTRAC for their CHMC and TSMC simulation components, respectively. They sampled the ICRU sphere using 1-cm-thick isocentric shells, and we present the results from their outermost shell. Based on their Monte Carlo simulations, they developed analytical formulas describing DNA damage yields as a function of LET and defined their reference radiation by taking the limit LET $\rightarrow$ 0.

For our data, all error bars and quoted uncertainties were obtained through propagation of the standard error on the mean ($SE = SD/\sqrt{n}$) for the mean yield values for neutrons $< Y_n >$ and photons $< Y_X >$. For each neutron energy, 100 statistically independent simulations were used. The uncertainties of the RBEs were dominated by statistical variations across photon runs; therefore 950 photon simulations were conducted.

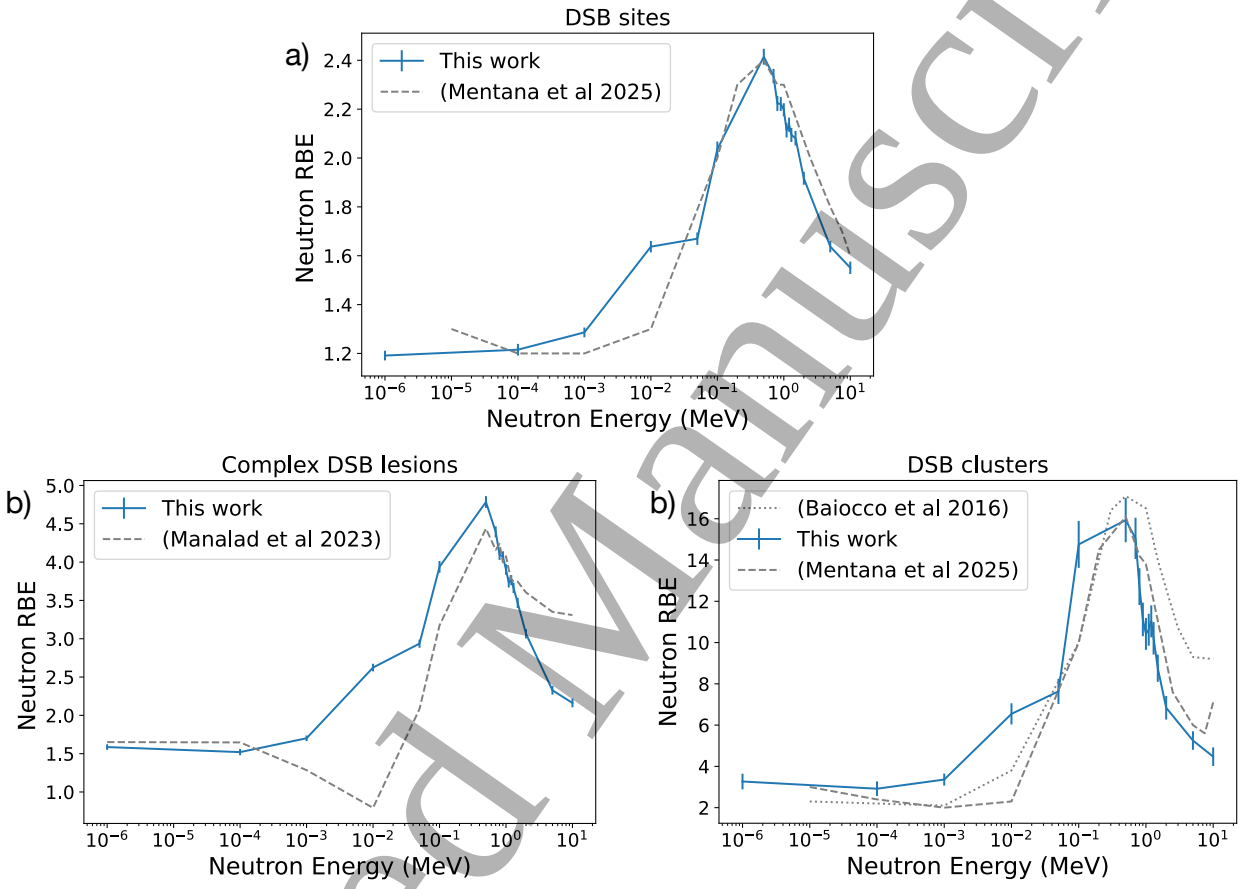

Figure 3: Comparison of neutron RBE values obtained in this study with literature results for pre-repair endpoints: (a) DSB sites, (b) Complex DSB lesions, and (c) DSB clusters. The three endpoints are detailed in Table 2. Results from (Baiocco *et al* 2016) were extracted using WebPlotDigitizer (Rohatgi 2024).

Following DNA damage simulations, our SDD files were subsequently processed using DaMaRiS to compute the RBE for misrepairs. Only one misrepair RBE curve is presented in this study, as we did not vary the already benchmarked NEHJ parameters provided in TOPAS-nBio. In Figure 4 a), we compare the RBE for misrepairs to the RBE for the pre-repair endpoints obtained in this study. In Figure 4 b), we compare the RBE for misrepairs to w_{R}, Q, and the RBE for DSB clusters from Baiocco *et al* (2016).

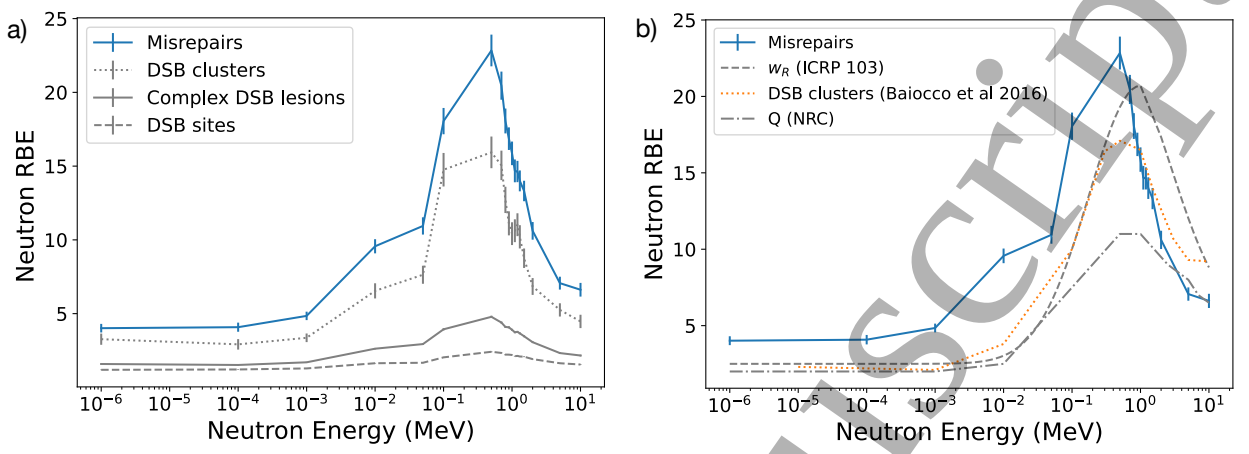

Figure 4: Misrepair results (a) Neutron RBE for misrepairs compared to the neutron RBE for various pre-repair endpoints. All the results in this panel were generated in this study. (b) Neutron RBE compared to the w_{R}, Q and the RBE for DSB clusters from Baiocco *et al* (2016). Values from (Baiocco *et al* 2016) were extracted using WebPlotDigitizer (Rohatgi 2024).

Figure 5 compares the neutron RBE curve for misrepairs obtained in this study with neutron maximal RBE (RBE_M) curves for various chromosomal aberrations reported in *in vitro* experiments from the literature. Schmid *et al* (2003) investigated dicentric chromosomes in human lymphocytes irradiated *in vitro* with nearly monoenergetic neutrons, with chromosome analysis performed in first-cycle metaphases. Our results are compared to their RBE values derived using 220 kV X-rays as the reference radiation.

Pandita and Geard (1996) examined chromosome aberrations induced in normal human fibroblasts by monoenergetic neutrons at the first mitosis post-irradiation. For their RBE calculations, they separated aberrations into three subgroups: (i) dicentrics and centric rings, (ii) interstitial deletions and acentric rings, and (iii) terminal deletions. To obtain an overall RBE for all aberration types combined, we summed the linear dose–response coefficients of these three subgroups for both neutrons and the ^{137}Cs reference radiation.

Similarly to Schmid *et al* (2003), Tanaka *et al* (1999) scored dicentric chromosomes in human lymphocytes irradiated with monoenergetic neutrons but only used ^{60}Co as a reference radiation.

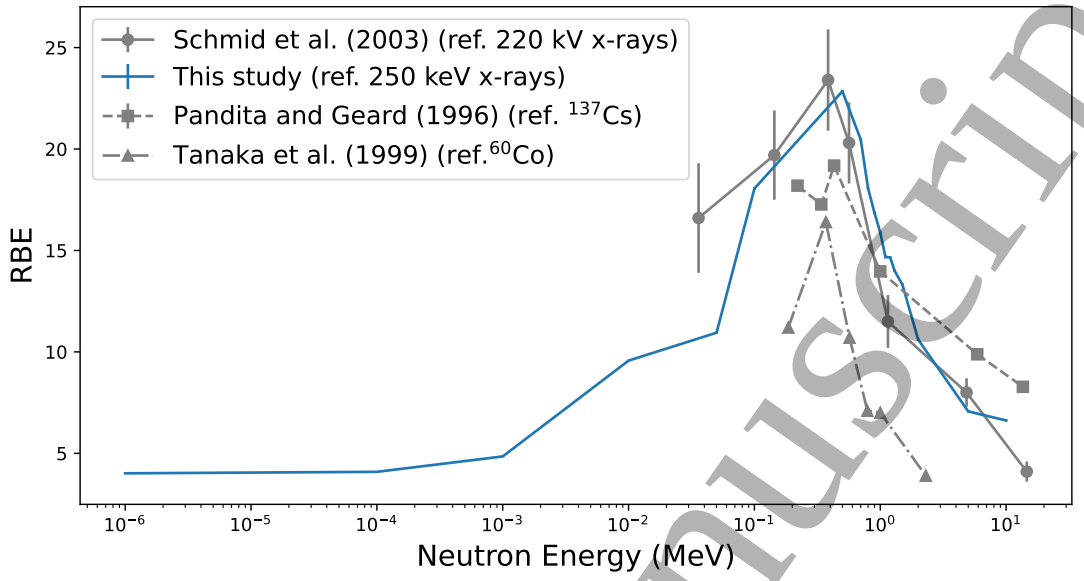

Figure 5: Comparing our simulated RBE for misrepairs to experimentally obtained neutron RBEs for various types of chromosomes aberrations. Ref. indicates the reference radiation used to compute the RBE, which for this study are 250 keV photons.

3.3 Nearby DSB pairs

The nearby DSB pair is a pre-repair endpoint, but the results pertaining to it are presented last because this endpoint was not used in prior work, and presenting the misrepair results first seemed more appropriate. In Figure 6 a), we provide the variation of the maximal RER as function of the maximal Euclidean distance selected to compute the yield of DSB pairs. By maximal RER, we mean the RER for a neutron energy of 0.5 MeV and we use RER here as opposed to RBE because the dose response becomes non-linear for DSB pairs separated by a large Euclidean distance, see Figure 2, and thus the ratio of yield is not equal to the RBE.

While Figure 6 a) shows the variation of the RER for nearby DSB pairs with Euclidean distance at a fixed energy of 0.5 MeV, Figure 6 b) shows the variation of the RBE (RER in the linear regime) for nearby DSB pairs with energy for a fixed Euclidean distance of 11 nm. The 11 nm Euclidean distance was selected to best match the misrepair RBE values in the high RBE region of the curve (around 0.5 MeV). Importantly, when considering the neutron and photon yields individually rather than their ratio, a distance of 11 nm does not reproduce the misrepair outcomes well. Instead, we find that the misrepair yields for 0.5 MeV neutrons and 250 keV x-rays are best matched using distances of 18 nm and 60 nm, respectively, see Figure 2.

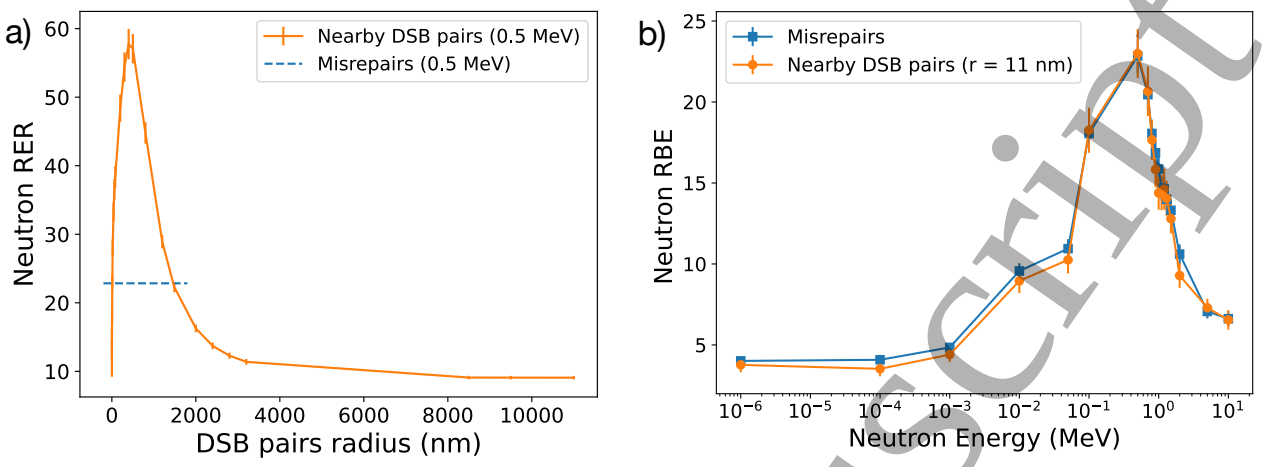

Figure 6: (a) Neutron RER for nearby DSB pairs as function of the Euclidean distance for 0.5 MeV neutrons. The plot is labeled RER because the the dose response is non-linear for DSB pairs with with a large Eucledian distance. b) RBE for misrepairs against the RBE for DSB pairs with a fix Euclidean distance of 11 nm.

4 Discussion

4.1 Dose response linearity

The approach taken in this study to compute the RBE relies on the assumption that the dose response relationships of the observed endpoints are linear. As shown in Figure 2 a), this assumption holds for the DSB pairs with the Euclidean distances of interest in this study, as well as for misrepairs. However, Figure 2 b) shows that for larger Euclidean distances, such as 300 nm, the dose response for DSB pairs is no longer linear up to 20 Gy. Consequently, had we used a repair model with a much larger interaction range, such as MEDRAS (Warmenhoven *et al* 2023), whose interaction half-width at half-maximum (HWHM) is 285.06 nm compared with 26.15 nm for DaMaRiS, we might have observed a non-linear dose response for misrepairs. In the following section on misrepairs, we provide evidence that DaMaRiS was an appropriate choice of repair model for our DNA damage simulation pipeline.

4.2 Comparing pre-repair endpoints across studies

In Fig. 3, we provide a comparison between the RBE curves obtained in this study and those obtained by Baiocco *et al* (2016), Manalad *et al* (2023), and Mentana *et al* (2025).

4.2.1 Comparison with Baiocco et al *(2016) and Mentana* et al *(2025)*

In the work of Baiocco *et al* (2016) and their subsequent study (Mentana *et al* 2025), the CHMC simulations were carried out with PHITS and the TSMC simulations PARTRAC (Friedland *et al* 2011), using a different nucleus model than the one used in this study; hence, differences in

the results are not unexpected. For the first step of the simulation pipeline, namely the CHMC simulations, the geometry used in this study was identical to that described in Baiocco *et al* (2016), consisting of spherical scoring volumes with a radius of r=1.5 cm. In the work of Mentana *et al* (2025), 1 cm-thick spherical shells were used instead, covering a narrower region by comparison. However, our results for both DSB sites and DSB clusters are in good agreement with those from Mentana *et al* (2025), and even better than with the results of Baiocco *et al* (2016) in the case of DSB clusters.

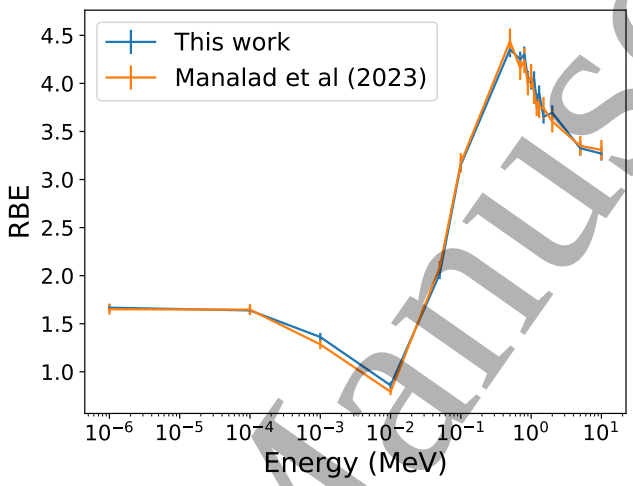

Figure 7: Comparison of the RBE curve for complex DSB lesions reported by Manalad *et al* (2023) with the curve obtained with the simulation pipeline used in this work, differing only by setting the TOPAS source parameter *BeamEnergySpectrumType* to "discrete," as in Manalad *et al* (2023).

4.2.2 Comparison with Manalad et al *(2023)*

The discrepancy between our previous RBE curve for complex DSB lesions presented in Manalad *et al* (2023) and the one presented in this study is entirely due to the *BeamEnergySpectrumType = "continuous"* parameter setting in TOPAS. Switching this parameter to *BeamEnergySpectrumType = "discrete"* yields the curve obtained by Manalad *et al* (2023), see Figure 7. For the TSMC simulations, the electrons, protons and alpha particles are sampled from energy distributions obtained with CHMC simulations. The parameter *BeamEnergySpectrumType = "discrete"* samples only the edges of the distribution bins, whereas the bins represent the likelihood of a range of energies and not a single point. This parameter change, which was justified *a priori*, makes the drop-off of the RBE curve steeper and results in better agreement with w_{R} and Q.

4.3 Comparing pre-repair endpoints obtained in this study

We now aim to compare the RBE associated with the various endpoints while maintaining all other parameters consistent. The definitions given to those endpoints allow them to have various numbers of basic lesions, but each must meet a minimum number of lesions which were listed in

Table 2. For the endpoints investigated in this study the maximal RBE increases with the required minimum number of basic lesions suggesting this could be a determining factor. This pattern can be observed across panels in Figure 3.

One possible explanation for that correlation is that the most basic form of an endpoint is the most likely form. In that case, the overall yield would be dominated by that form and because neutrons yield more complex lesions than photons, the RBE would increase with increasing level of required minimal complexity. In other words, the idea suggested here is that even if the definition of an endpoint allows for very complex lesions, such as is the case with the Complex DSB lesion from Manalad *et al* (2023), it is its most basic form that will dictate the RBE and not how complex the endpoint can be.

4.4 Misrepairs

Peaking at an RBE value of 23(1) for neutrons of 0.5 MeV, the RBE for misrepairs exceeds the RBE of the complex DSB lesions, DSB clusters, and DSB sites. Even though, our simulation parameters do not best match the experimental parameters of the studies introduced with Figure 5, the RBE results we obtained show some agreements with the experimental results, especially with that of Schmid *et al* (2003), thus providing experimental support to the simulation results.

An accurate classification of specific chromosome aberration subclasses, such as chromosomal exchanges, large scale rearrangements, or small insertions and deletions, would require a detailed and experimentally validated reconstruction of chromosome territory geometry. At present, such high fidelity modeling is not available; consequently, our simulation framework would not yield reliable subtype specific aberration frequencies. Although the approach adopted here does not distinguish among individual aberration classes, it remains informative in the context of carcinogenesis. It is generally accepted that unstable aberrations, including dicentrics and large acentric fragments, are often eliminated through mitotic failure and therefore contribute less to long term clonal persistence, whereas stable aberrations, particularly balanced translocations, can be propagated through many cell divisions and have the potential to initiate or promote malignant transformation when they alter gene regulation or create oncogenic fusion genes.

The misrepair endpoint used in this study therefore captures a broad spectrum of DNA end joining errors, including those with established or suspected carcinogenic potential. While accurately resolving the various aberration subclasses could in principle yield endpoints more directly linked to carcinogenesis or cell kill, the relationship between specific aberration types and cancer risk is itself an active area of investigation. For example, the work by MacKinnon and Campbell (2011) suggests that dicentrics may play a more significant role in carcinogenic processes than previously assumed.

DaMaRiS currently supports two repair configurations: one that includes only NHEJ and another that combines NHEJ with HR. Because our cell model is intended to represent cells in the G0/G1 phase, where HR is not active, we opted for the NHEJ only pathway. Introducing HR would likely reduce the overall yield of misrepair. However, it is not obvious whether HR would preferentially decrease the misrepair yield for photons or neutrons, or instead reduce both proportionally. As

a result, the impact of HR on simulation RBE estimates is not straightforward to predict. The same logic apply for other repair pathways such as alt-NHEJ which is more prone to error than NEHJ. Experimental data indicate that cell cycle related variations in radiosensitivity are more pronounced for x-rays than for neutrons. We therefore think neutron RBE may be lower in the G2/M stages. Understanding how and if the dynamic of different repair pathways contributes to this behavior would be an important direction for future work.

For the development of the DaMaRiS toolkit, DNA damage simulations were needed; therefore, the kinetics of the repair models used by DaMaRiS are inherently influenced by the DNA damage simulation used in its development. The effects of compensatory mechanisms in repair models due to the choice of DNA damage simulation tools are discussed at length in Warmenhoven *et al* (2023). Notably, the authors demonstrate that DNA damage simulation tools resulting in more clustered damage lead to repair models that restrict the range over which DSB ends interact. Two repair simulation tools can produce the same final results using different kinetics, provided they are coupled with the DNA damage tool with which they were benchmarked. To demonstrate how our DNA damage simulation tool compares to the one used to benchmark DaMaRiS, Figure 8 compares the benchmarking results obtained by Manalad *et al* (2023) to those obtained with the DNA damage simulation tool used in the development of DaMaRiS, as published in Warmenhoven *et al* (2023). The agreement between these results suggests that coupling our DNA damage model with the DaMaRiS toolkit should yield accurate outcomes.

Briefly, the DaMaRiS algorithm used in this study first initiate DSB ends within the cell boundary. The ends are then allowed to move randomly and independently of each other in a sub-diffusive manner. When two DSB ends come within 25 nm of each other, they can interact to form a synaptic complex and potentially permanently bind, resulting in either a repair or a misrepair.

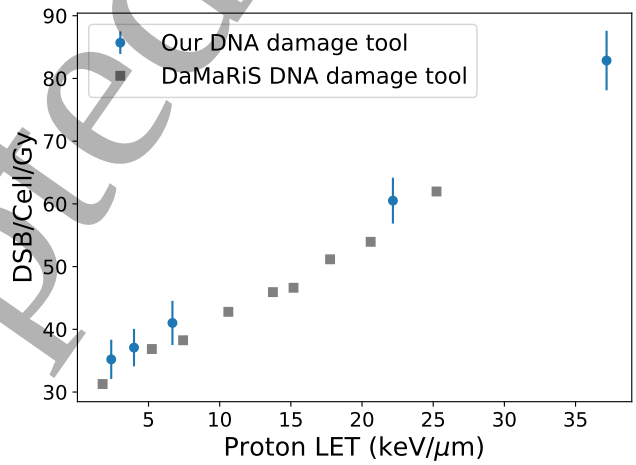

Figure 8: Comparing the DSB yield per cell per gray against proton LET for our DNA damage simulation tool (Manalad *et al* 2023) to the the the one used to benchmark DaMaRiS (Warmenhoven *et al* 2023). The data from (Warmenhoven *et al* 2023) were extracted using WebPlotDigitizer (Rohatgi 2024) and, therefore, are presented without error bars in this work.

4.5 Nearby DSB pairs

By varying the maximum Euclidean distance used to compute the nearby DSB pairs we found that 11 nm results in an RBE for nearby DSB pairs that best matches the RBE obtained for misrepairs. We will now seek to provide a rationale for the shape of the curve for the maximal RER as function of Euclidean distances provided in Figure 6 a). The y-axis is labeled RER in this case as opposed to RBE because over large distances the linearity of the dose response for nearby DSB pairs does not hold anymore, and therefore, the RBE and RER are not equivalent.

For a given irradiation condition, the variation in both the neutron and photon nearby DSB pair yields (Y_n and Y_X) with respect to Euclidean distance follows sigmoid curves. The plateau of these sigmoid curves is given by the combination $C(n_{\mathrm{DSB}}, 2)$, which represents the number of all possible pairs that can be formed from the DSBs present in the cell. The shape of Figure 6 a) is, therefore, the ratio of two sigmoids. For a single irradiation, the horizontal asymptote seen in Figure 6 a) is given by the ratio of $C(n_{\mathrm{DSB}}, 2)_n$ to $C(n_{\mathrm{DSB}}, 2)_x$; however, this asymptote cannot be computed using the mean DSB yield from neutron and photon irradiation repeats, because $C(n_{\mathrm{DSB}}, 2)$ is not a linear operation.

This finding is included in this article even though its significance is uncertain or possibly null. The RBE is, by definition, a ratio of two outcomes. From the RER curve in Fig. 6 a), we see that for any maximum RBE in the range of 10 to 60, one could select a Euclidean distance that provide the correct ratio to reproduce it. However, when examining the neutron and photon yields individually rather than their ratio, a distance of 11 nm does not correlate well with the misrepair outcomes. Instead, we observe that the misrepair yields for 0.5 MeV neutrons and 250 keV x-rays are best matched by distances of 18 nm and 60 nm, respectively, see Figure 2. Taking the ratio of these two outcomes yields a curve that closely matches the RBE for misrepairs. Now this is not a RBE, because by definition the RBE is a ratio of dose for the same endpoints. Those results suggest that difference in lesions pattern could affect the repair dynamics and thus shed some doubts on the common approach of *in silico* experiments that consists of using the same pre-repair endpoint for all radiation qualities as a proxy for larger scale genomic alterations.

4.6 Other remarks

The values of w_{R} and Q at very low neutron energies are approximately 2.5 for w_{R} and 2 for Q. In contrast, the RBE obtained for misrepairs at very low energies is around 4. This discrepancy could be partly explained by the fact that we are examining only the outer portion of the ICRU-4 sphere rather than RBE values for its entirety. In the work of Baiocco *et al* (2016), Montgomery *et al* (2021), and Manalad *et al* (2023), the outer scoring volume consistently shows the highest RBE at low neutron energies among all scoring volumes. Furthermore, some experimental studies on neutron RBE at low energies suggest that the current radioprotection system may underestimate neutron RBE in this range (Paterson *et al* 2022). Finally, the curves obtained in this work are endpoint-specific RBE curves and are therefore not directly comparable to w_{R} and Q, which were compiled from multiple types of data.

A major limitation for the study of neutron RBE with Geant4-DNA at the moment is the absence

of models for low-energy heavy ion transport. Oxygen, nitrogen and carbon makes up 3.3 % of the dose at 0.5 MeV and 9.2 % of the does at 10 MeV (Lund *et al* 2020). However, this issue can be easily addressed once GEANT4-DNA physics lists capable of handling low-energy heavy ions are made available.

5 Conclusion

In this study, we employed Monte Carlo simulations to investigate neutron RBE for both pre-DNA repair and post-DNArepair endpoints. To the best of our knowledge, this represents the first *in silico* study to present RBE estimates for misrepairs, and DSB clusters based on Euclidean distances from both the direct and indirect effects of ionizing radiation. This was achieved by modifying our previously-published DNA damage simulation pipeline to ensure compatibility with the SDD format, enabling seamless integration with the repair simulation toolkit DaMaRiS as well as with a novel in-house clustering algorithm.

The neutron RBE for misrepairs that we obtained exhibits a higher peak compared to previously published pre-repair endpoints. We were able to closely reproduce the RBE for misrepairs with the RBE for nearby DSB pairs with a maximum distance of 11 nm; however, the damage yields themselves were best matched by DSB pairs with a maximum Euclidean distance of 18 nm and 60 nm for 0.5 MeV neutrons and 250 keV photons, respectively. While the ability of DSB pair yields to better match those of misrepairs than previously investigated pre-repair endpoints may suggest that the structures of radiation-induced DNA damage leading to wrong-end joining are better captured by DSB clusters defined with Euclidean distances rather than by base pair distances along the genome, the fact that the maximal Euclidean distances that best match neutron and photon misrepair yields are different casts some doubt on the practice of using a single pre-repair endpoint that serves as a good predictor of larger-scale aberrations for all radiation qualities.

This study lays the groundwork for refining simulation techniques, which will, in turn, enhance our fundamental understanding of the stochastic risks associated with exposure to neutron radiation. However, it does not yet provide a fully accurate assessment of neutron RBE, highlighting the need for ongoing research and development in this area.

6 Acknowledgements

2 We are grateful to Chris Lund, Logan Montgomery, James Manalad, and Felix Mathew for their invaluable contributions to this research project. We extend special thanks to Chris Lund for providing access to the neutron secondary particle spectra, which is an integral part of this project's pipeline. We also thank Logan Montgomery and James Manalad for sharing their TOPAS scorer and geometry, which were integral to the development of this work. Finally, we are thankful to Felix Mathew and James Manalad for their ongoing support and insightful feedback throughout the project, and to Luc Galarneau for laboratory administration support. This research was made possible in part through computational resources provided by Calcul Québec and the Digital Research Alliance of Canada.

Funding for this research was provided by the Collaborative Research and Training Experience grant entitled Responsible Health and Healthcare Data Science (SDRDS) of the Natural Sciences and Engineering Research Council, The Canada Foundation for Innovation John R. Evans Leaders Fund, the Canadian Space Agency Grant #19FAMCGB25 held by JK, a Discovery Grant of Natural Sciences and Engineering Research Council of Canada held by JK, and a Fonds de recherche du Québec – Nature et technologies Masters Training Award received by ND.

Additionally we gratefully acknowledge the following open-source softwares: Geant4 (Agostinelli *et al* 2003), Geant4-DNA (Incerti *et al* 2010b,c, Bernal *et al* 2015, Incerti *et al* 2018, Tran *et al* 2024), TOPAS (Perl *et al* 2012), TOPAS-nBio (Schuemann *et al* 2019a), DaMaRiS (Warmenhoven *et al* 2019), WebPlot Digitizer (Rohatgi 2024), NumPy (Harris *et al* 2020) and Matplotlib (Hunter 2007)

References

Agostinelli S *et al* 2003 Geant4—a Simulation Toolkit *Nuclear Instruments and Methods in Physics Research Section A: Accelerators, Spectrometers, Detectors and Associated Equipment* **506**(3) 250–303
URL http://dx.doi.org/10.1016/S0168-9002(03)01368-8

Baiocco G *et al* 2016 The origin of neutron biological effectiveness as a function of energy *Scientific Reports* **6** 34033
URL http://dx.doi.org/10.1038/srep34033

Bernal M *et al* 2015 Track Structure Modeling in Liquid Water: A Review of the Geant4-DNA Very Low Energy Extension of the Geant4 Monte Carlo Simulation Toolkit *Physica Medica* **31**(8) 861–874
URL http://dx.doi.org/10.1016/j.ejmp.2015.10.087

CIRRPC 1995 Neutron quality factor Technical Report ORAU-95/F-29 Oak Ridge Inst. for Science and Education
URL http://dx.doi.org/10.2172/114580

Friedland W, Dingfelder M, Kundrát P and Jacob P 2011 Track structures, DNA targets and radiation effects in the biophysical Monte Carlo simulation code PARTRAC *Mutation Research - Fundamental and Molecular Mechanisms of Mutagenesis* **711**(1-2) 28–40
URL http://dx.doi.org/10.1016/j.mrfmmm.2011.01.003

Goldhagen P 2000 Overview Of Aircraft Radiation Exposure And Recent Er-2 Measurements: *Health Physics* **79**(5) 526–544
URL http://dx.doi.org/10.1097/00004032-200011000-00009

Harris C R *et al* 2020 Array programming with NumPy *Nature* **585**(7825) 357–362
URL http://dx.doi.org/10.1038/s41586-020-2649-2

Henthorn N T, Warmenhoven J W, Sotiropoulos M, Mackay R I, Kirkby N F, Kirkby K J and Merchant M J 2018 In Silico Non-Homologous End Joining Following Ion Induced DNA Double Strand Breaks Predicts That Repair Fidelity Depends on Break Density *Scientific Reports* **8**(1) 2654
URL http://dx.doi.org/10.1038/s41598-018-21111-8

Howell R M, Hertel N E, Wang Z, Hutchinson J and Fullerton G D 2006 Calculation of effective dose from measurements of secondary neutron spectra and scattered photon dose from dynamic MLC IMRT for 6 MV, 15 MV, and 18 MV beam energies *Medical Physics* **33**(2) 360–368
URL http://dx.doi.org/10.1118/1.2140119

Hunter J D 2007 Matplotlib: A 2D graphics environment *Computing in Science & Engineering* **9**(3) 90–95
URL http://dx.doi.org/10.1109/MCSE.2007.55

ICRP 2003 ICRP 92: Relative Biological Effectiveness (RBE), Quality Factor (Q), and Radiation Weighting Factor (wR) *Annals of the ICRP* **33**(4)
URL http://dx.doi.org/10.1016/s0146-6453(03)00024-1

ICRP 2007 ICRP 103: The 2007 Recommendations of the ICRP *Annals of the ICRP* **37**(2-4)
URL http://dx.doi.org/10.1016/j.icrp.2007.10.003

Incerti S *et al* 2010a The Geant4-DNA project *International Journal of Modeling, Simulation, and Scientific Computing* **1**(2) 157–178
URL https://doi.org/10.1142/S1793962310000122

Incerti S *et al* 2010b THE GEANT4-DNA PROJECT *International Journal of Modeling, Simulation, and Scientific Computing* **01**(02) 157–178
URL http://dx.doi.org/10.1142/s1793962310000122

Incerti S, Douglass M, Penfold S, Guatelli S and Bezak E 2016 Review of Geant4-DNA applications for micro and nanoscale simulations *Physica Medica* **32**(10) 1187–1200
URL http://dx.doi.org/10.1016/j.ejmp.2016.09.007

Incerti S *et al* 2010c Comparison of GEANT4 Very Low Energy Cross Section Models with Experimental Data in Water *Medical Physics* **37**(9) 4692–4708
URL http://dx.doi.org/10.1118/1.3476457

Incerti S *et al* 2018 Geant4-DNA example applications for track structure simulations in liquid water: A report from the Geant4-DNA Project *Medical Physics* **45**(8) e722–e739
URL http://dx.doi.org/https://doi.org/10.1002/mp.13048

Ingram S P, Warmenhoven J W, Henthorn N T, Smith E A K, Chadwick A L, Burnet N G and Mackay R I e a 2019 Mechanistic modelling supports entwined rather than exclusively competitive DNA double-strand break repair pathway *Scientific Reports* **9**(1) 6359
URL http://dx.doi.org/10.1038/s41598-019-42901-8

Jeggo P A and Löbrich M 2007 DNA double-strand breaks: their cellular and clinical impact? *Oncogene* **26**(56) 7717–7719
URL http://dx.doi.org/10.1038/sj.onc.1210868

Lund C M, Famulari G, Montgomery L and Kildea J 2020 A microdosimetric analysis of the interactions of mono-energetic neutrons with human tissue *Physica Medica* **73** 29–42
URL http://dx.doi.org/10.1016/j.ejmp.2020.04.001

MacKinnon R N and Campbell L J 2011 The Role of Dicentric Chromosome Formation and Secondary Centromere Deletion in the Evolution of Myeloid Malignancy **2011** 1–11
URL http://dx.doi.org/10.4061/2011/643628

Manalad J, Montgomery L and Kildea J 2023 A study of indirect action's impact on simulated neutron-induced DNA damage **68**(7) 075014
URL http://dx.doi.org/10.1088/1361-6560/acc237

Mentana A *et al* 2025 Mapping neutron biological effectiveness for DNA damage induction as a function of incident energy and depth in a human sized phantom *Scientific Reports* **15**(1) 2209
URL http://dx.doi.org/10.1038/s41598-025-85879-2

Montgomery L, Lund C M, Landry A and Kildea J 2021 Towards the characterization of neutron carcinogenesis through direct action simulations of clustered DNA damage *Physics in Medicine & Biology* **66**(20) 205011
URL http://dx.doi.org/10.1088/1361-6560/ac2998

Ottolenghi A, Smyth V and Trott K 2013 Assessment of cancer risk from neutron exposure – The ANDANTE project *Radiation Measurements* **57** 68–73
URL http://dx.doi.org/https://doi.org/10.1016/j.radmeas.2012.10.017

Pandita T K and Geard C R 1996 Chromosome aberrations in human fibroblasts induced by monoenergetic neutrons. I. Relative biological effectiveness *Radiat. Res.* **145**(6) 730–739

Paterson L C *et al* 2022 High-Accuracy Relative Biological Effectiveness Values Following Low-Dose Thermal Neutron Exposures Support Bimodal Quality Factor Response with Neutron Energy *International Journal of Molecular Sciences* **23**(2) 878
URL http://dx.doi.org/10.3390/ijms23020878

Perl J, Shin J, Schümann J, Faddegon B and Paganetti H 2012 TOPAS: An innovative proton Monte Carlo platform for research and clinical applications *Medical Physics* **39**(11) 6818–6837
URL http://dx.doi.org/10.1118/1.4758060

Rohatgi A 2024 WebPlotDigitizer
URL https://automeris.io

Sato T *et al* 2013 Particle and heavy ion transport code system, PHITS, version 2.52 *Journal of Nuclear Science and Technology* **50**(9) 913–923
URL http://dx.doi.org/10.1080/00223131.2013.814553

Schmid E, Schlegel D, Guldbakke S, Kapsch R P and Regulla D 2003 RBE of nearly monoenergetic neutrons at energies of 36 keV-14.6 MeV for induction of dicentrics in human lymphocytes *Radiat. Environ. Biophys.* **42**(2) 87–94

Schneider U and Hälg R 2015 The Impact of Neutrons in Clinical Proton Therapy *Frontiers in Oncology* **5**
URL http://dx.doi.org/10.3389/fonc.2015.00235

Schuemann J, McNamara A L, Ramos-Méndez J, Perl J, Held K D, Paganetti H, Incerti S and Faddegon B 2019a TOPAS-nBio: An Extension to the TOPAS Simulation Toolkit for Cellular and Sub-cellular Radiobiology *Radiation Research* **191**(2) 125–138
URL http://dx.doi.org/10.1667/rr15226.1

Schuemann J *et al* 2019b A New Standard DNA Damage (SDD) Data Format *Radiation Research* **191**(1) 76–92
URL http://dx.doi.org/10.1667/rr15209.1

Stricklin D L, VanHorne-Sealy J, Rios C I, Scott Carnell L A and Taliaferro L P 2021 Neutron Radiobiology and Dosimetry *Radiation Research* **195**(5) 480–496
URL http://dx.doi.org/10.1667/RADE-20-00213.1

Tanaka K, Gajendiran N, Endo S, Komatsu K, Hoshi M and Kamada N 1999 Neutron Energy-Dependent Initial DNA Damage and Chromosomal Exchange *Journal of Radiation Research* **40**(Suppl) S36–S44
URL http://dx.doi.org/10.1269/jrr.40.S36

Tran H N *et al* 2024 Review of Chemical Models and Applications in Geant4-DNA: Report from the ESA BioRad III Project *Medical Physics* **51**(9) 5873–5889
URL http://dx.doi.org/10.1002/mp.17256

US NRC 2021 Units of Radiation Dose *Code of Federal Regulations* **10**(20.1004) 298–300
URL https://www.nrc.gov/reading-rm/doc-collections/cfr/part020/part020-1004.html

Warmenhoven J W, Henthorn N T, Ingram S P, Chadwick A L, Sotiropoulos M and Korabel N e a 2019 Insights into the non-homologous end joining pathway and double strand break end mobility provided by mechanistic in silico modelling *DNA Repair (Amst)* **85** 102743
URL http://dx.doi.org/10.1016/j.dnarep.2019.102743

Warmenhoven J W *et al* 2023 Effects of Differing Underlying Assumptions in In Silico Models on Predictions of DNA Damage and Repair *Radiation Research* **200**(6) 509–522
URL http://dx.doi.org/10.1667/RADE-21-00147.1

White D R, Booz J, Griffith R V, Spokas J J and Wilson I J 1989 ICRU Report 44: Tissue Substitutes in Radiation Dosimetry and Measurement *Journal of the International Commission on Radiation Units and Measurements* **os23**(1)
URL http://dx.doi.org/10.1093/jicru/os23.1.report44

Zabihi A, Tello J, Incerti S, Francis Z, Forozani G, Semsarha F, Moslehi A and Bernal M A 2020 Determination of fast neutron RBE using a fully mechanistic computational model *Applied Radiation and Isotopes* **156** 108952
URL http://dx.doi.org/10.1016/j.apradiso.2019.108952